Bound magnetic polarons in p-type $Cu_2Mn_{0.9}Zn_{0.1}SnS_4$

G. H. McCabe, T. Fries, M. T. Liu, and Y. Shapira
Department of Physics and Astronomy, Tufts University, Medford, Massachusetts 02155

L. R. Ram-Mohan
Department of Physics, Electrical and Computer Engineering, Worcester Polytechnic Institute, Worcester, Massachusetts 01609

R. Kershaw* and A. Wold
Department of Chemistry, Brown University, Providence, Rhode Island 02912

C. Fau and M. Averous
Group d'Etude des Semiconducteurs URA 357, Université Montpellier II, Place Eugene Bataillon, 34095 Montpellier Cedex 5, France

E. J. McNiff, Jr.
Francis Bitter National Magnet Laboratory, Massachusetts Institute of Technology, Cambridge, Massachusetts 02139
(Received 7 April 1997; revised manuscript received 20 May 1997)

Bound magnetic polarons (BMP's) in p-type $Cu_2Mn_{0.9}Zn_{0.1}SnS_4$ were investigated using magnetization measurements. The magnetization M was studied from 2 to 60 K in magnetic fields up to 55 kOe. The data show the characteristic features of BMP's in the collective regime. In addition, the onset of antiferromagnetic order in the ''matrix'' surrounding the BMP's leads to anomalies in the BMP susceptibility at the Néel temperature of the matrix $T_N = 8$ K. Below 15 K the low-field magnetization of the BMP's is quite anisotropic. A detailed analysis of the isothermal magnetization curves, based on Wolff's work but with some additional assumptions, separates the BMP contributions to M from the contribution of the matrix. The analysis gives the spontaneous moment m_s of a single BMP as a function of temperature T, and the concentration N of BMP's. The value $m_s = 143$ Bohr magnetons/BMP at the lowest temperatures is consistent with the expected radius of the hole orbit, of order 10 Å. The observed T dependence of m_s is compared with theoretical calculations based on a model that assumes that the wave function in the absence of the p-d interaction is hydrogenic. The calculated decrease of m_s with increasing T is somewhat slower than that deduced from the experimental data. The BMP concentration N, from an analysis of the magnetization data, is about 2×10^{19} BMP/cm^3 in all the samples. This N is consistent with the observed hopping conductivity at low temperatures. High-field magnetization data, up to 300 kOe, show the canted-to-paramagnetic phase transition of the matrix. At 1.4 K the transition is near 225 kOe. [S0163-1829(97)01235-6]

I. INTRODUCTION

The characteristic features of magnetic semiconductors[1] and of dilute magnetic semiconductors[2,3] arise from the sp-df interaction. This interaction couples the spins of s-like electrons and p-like holes near the band edges to the d- or f-shell spins of the transition ions. When donors or acceptors are present, the sp-df interaction often leads to the formation of bound magnetic polarons (BMP's). A BMP is a particular type of complex near an occupied donor or an acceptor. It consists of the bound electron (hole) together with the spins of the transition ions within the Bohr orbit. Due to the sp-df interaction the latter spins can have a significant net ferromagnetic alignment, in which case the BMP resembles a ''ferromagnetic bubble'' embedded in a matrix of transition ions that surround it.

The early research on BMP's was carried out some 20–30 years ago, mainly on the Eu chalcogenides, which are the best-known magnetic semiconductors. Among the earliest works were the experiments of von Molnar and Methfessel[4] and the theories of Yanase and Kasuya[5] and Nagaev.[6] These were followed by many experiments (e.g., Refs. 7–11) and theoretical treatments (e.g., Refs. 12–14). More recent works on BMP's in bulk materials focused on II-VI dilute magnetic semiconductors (DMS's).[15–17] These recent works were reviewed by Wolff.[18]

The recent works on DMS's showed that appreciable BMP effects may be observed even when the time-averaged ferromagnetic alignment of the d spins in the BMP is very weak. The reason is that the *instantaneous* magnetic moment may still be appreciable due to fluctuations about the time-averaged value. This is a consequence of the finite number of d spins within the Bohr orbit. The case of a weak time-averaged BMP magnetic moment is therefore called the ''fluctuation regime.''

On the other hand, when the time-averaged BMP magnetic moment is appreciable (compared to the net saturation moment of all the spins in the Bohr orbit) one speaks of the ''collective regime.'' The fluctuation regime occurs at relatively high temperatures and the collective regime at low temperatures. The temperature where the smooth transition between the two regimes occurs is governed by several parameters.[18] The BMP's observed in the early studies of the Eu chalocogenides[7–11] were in the collective regime. On the

 © 1997 The American Physical Society

other hand, BMP's in *n*-type II-VI DMS's are usually in the fluctuation regime because the collective regime is reached only below ~ 1 K.[16–18]

Conditions for observing BMP's in the collective regime are very favorable in *p*-type Mn-based DMS's having the stannite or wurtz-stannite crystal structures.[19] The antiferromagnetic (AF) interaction between the Mn^{2+} spins is greatly reduced in these crystal structures,[20] which facilitates the alignment of the Mn spins within the Bohr orbit. In addition, the binding energy for acceptor BMP's in these materials is much larger than for donor BMP's. One reason is that Bohr radius for holes is smaller. Another reason is that the *p-d* exchange constant β for holes is much larger than the *s-d* exchange constant α for electrons. The collective regime in *p*-type DMS with the stannite structure may extend up to 100 K or even higher temperatures.[19]

Pure Cu_2MnSnS_4 has the stannite crystal structure and it orders antiferromagnetically at 8.8 K.[20] The present work is on BMP's in *p*-type $Cu_2Mn_{0.9}Zn_{0.1}SnS_4$. This DMS also has the stannite structure. The focus of the work is on the collective regime. Although this regime of BMP behavior was previously studied in a few materials,[7,9,21,22] there was only one previous study of the magnetic behavior over a wide temperature range.[23] The magnetization at temperatures somewhat above the collective regime was studied by Wojtowicz *et al.* using the photomemory effect.[24]

In the present work the BMP magnetization was measured over the temperature range $2 \leqslant T \leqslant 60$ K. A detailed analysis yielded the BMP spontaneous magnetic moment $m_s(T)$ and the concentration N of BMP's. The results for $m_s(T)$ were compared with detailed theoretical calculations. The magnetic behavior of the Mn ions in the matrix outside the BMP's was also studied. The latter behavior is compared with the behavior of a Cu_2MnSnS_4 sample with no BMP's.[20] Some electrical transport data for $Cu_2Mn_{0.9}Zn_{0.1}SnS_4$ are also presented. They support the existence of acceptor BMP's in this material.

II. EXPERIMENT

Three single crystals of $Cu_2Mn_xZn_{1-x}SnS_4$, called samples *A*, *B*, and *C*, were studied. They were grown by the Bridgman method under very similar conditions. All three crystals had a nominal Mn concentration $x = 0.9$. (Note that this x refers to the fraction of *divalent* cations that are Mn.) The actual Mn concentration was determined only for sample *A*, using the high-field saturation magnetic moment. A comparison of this saturation moment with that of Cu_2MnSnS_4 gave $x = 0.88$. A slightly lower value for the same sample, $x = 0.85$, was obtained from a comparison of the Curie constant with that of Cu_2MnSnS_4. The value from the saturation moment was considered to be more accurate. The magnetic behavior of all three samples in fields up to 55 kOe was very similar, but only sample *A* was studied at higher fields.

The magnetization was measured using the equipment described in Ref. 20. Samples *A* and *B* were oriented by x rays and magnetization data for them were taken with the magnetic field **H** both parallel and perpendicular to the *c* axis. Sample C was not oriented and its magnetization was measured only for one field direction.

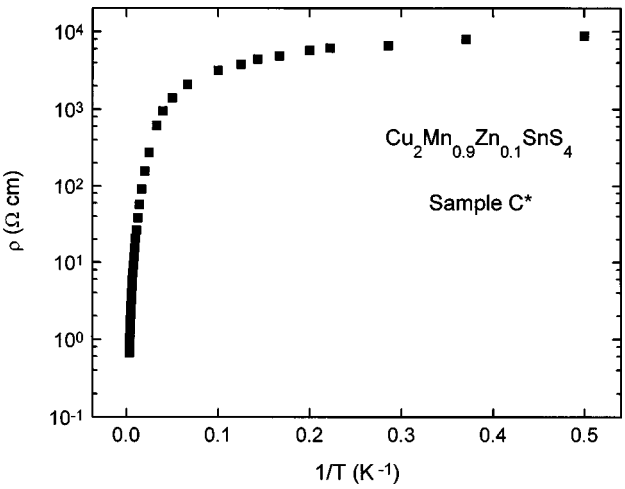

FIG. 1. Temperature dependence of the resistivity ρ of plate C^*.

Resistivity data were taken on an unoriented plate that was cut from the same boule as same C. This plate will be called C*. The plate was 380 μm thick and the other linear dimensions were several millimeters. Electrical contacts were made with indium. The resistivity was measured with the van der Paw method using dc current.

III. ELECTRICAL TRANSPORT

The sign of the thermoelectric power was determined at room temperature. The results showed that all samples (*A*, *B*, *C*, and the plate C*) were *p* type. Attempts to obtain the hole concentration from Hall measurements on plate C* were unsuccessful, presumably because the mobility was low.

The resistivity ρ was measured from 350 to 2 K. The results, plotted as a function of $1/T$, are shown in Fig. 1. The behavior at the higher temperatures is typical for a gradual freezing out of the carriers with decreasing T. At lower temperatures the behavior is characteristic of hopping conduction.[25] The hole binding energy E_b near room temperature was estimated from the nearly linear variation of $\ln(\rho)$ with $1/T$ in this temperature region. The result was $E_b \cong 95$ meV, with an uncertainly of about 10%.

The behavior in Fig. 1 indicates that the acceptor concentration N is lower than the critical concentration N_c at the metal-insulator transition. The usual Mott estimate of N_c is, in terms of the effective Bohr radius a_0^*,

$$N_c \cong (0.26/a_0^*)^3. \tag{1}$$

A typical value for acceptors in II-VI semiconductors is $a_0^* = 10$ Å, which leads to $N_c \cong 2 \times 10^{19}$ cm^{-3}. This value does not include the effect of the *p-d* interaction on the hole orbit in the BMP. The hole wave function in a BMP is ''pulled in,'' so that the effective hole radius is smaller than in the absence of the *p-d* interaction. Starting from a simple hydrogenic model for the acceptor, the shape of the hole wave function in the BMP does not remain exactly hydrogenic.[19] Nevertheless, a rough idea of the shrinking of the hole orbit may be obtained by focusing on the peak in the radial probability density $4\pi r^2 |\phi|^2$. The calculations presented below indicated that when T is of order 10 K, or

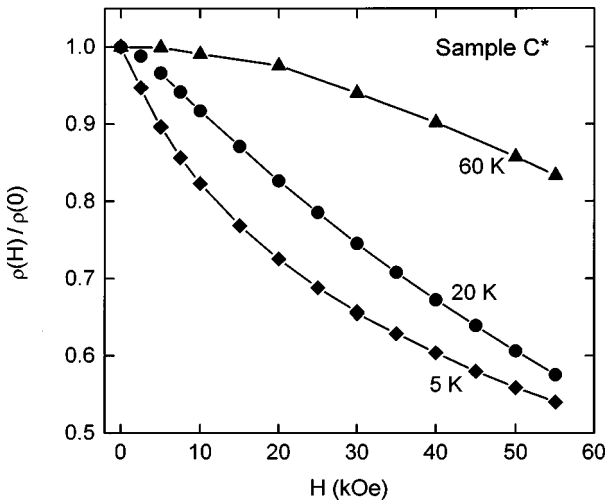

FIG. 2. Magnetoresistance of plate C^* at several temperatures.

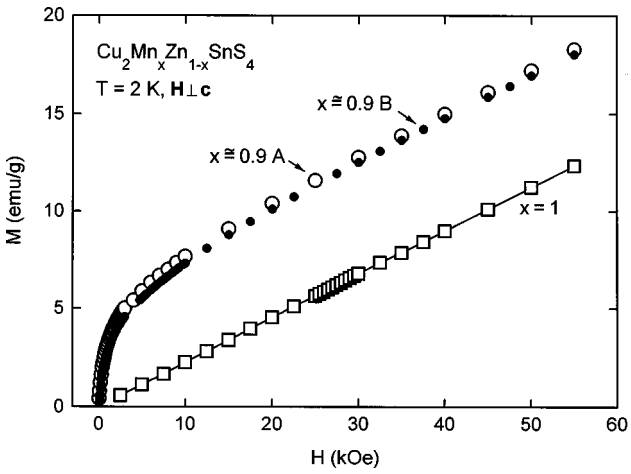

FIG. 3. Magnetization of samples A and B (both with $x \cong 0.9$) at 2 K. Also shown, for comparison, is the magnetization of a sample with $x=1$ and with no BMP's (Ref. 20). In all cases the magnetic field **H** is perpendicular to the c axis.

lower, this peak is near $0.65a_0^*$, compared to a_0^* in the hydrogenic model. On this basis, the estimate for N_c should change to about 7×10^{19} cm^{-3}. The data in Fig. 1 suggest therefore that the actual acceptor concentration N in sample C^* was lower than $\sim10^{20}$ cm^{-3}. As discussed later, the analysis of the magnetization data for samples A, B, and C led to acceptor concentrations $N\cong2\times10^{19}$ cm^{-3}.

Magnetoresistance (MR) data are shown in Fig. 2. These data were taken with **H** in the plane of the C^* plate, but other data at 9 kOe showed that the MR was not sensitive to field direction. The negative MR in Fig. 2 is typical for hopping conduction involving BMP's.[8,10,11] With increasing H, the Mn spins outside the BMP become increasingly more parallel and the difference between the magnetization inside and outside the BMP decreases. One of the consequences is that the hole orbit in the BMP expands with increasing H, leading to an increase in the hopping conduction. The magnitude of the MR decreases with increasing T because for a given H the alignment of the Mn spins outside the BMP is weaker at higher T.

IV. MAGNETIZATION

A. Characteristic magnetization of BMP's in the collective regime

Figure 3 compares the low-temperature magnetization M of samples A and B ($x\cong0.9$) with that of Cu_2MnSnS_4 ($x=1$). The Cu_2MnSnS_4 sample was studied in Ref. 20. All the data in Fig. 3 were taken at 2 K, with $\mathbf{H}\perp\mathbf{c}$. The most significant feature is the fast rise of M at low H for samples A and B. The fast rise does not occur in Cu_2MnSnS_4. A fast magnetization rise at low H was also observed at 2 K when samples A and B were measured in the configuration $\mathbf{H}\|\mathbf{c}$, and also in sample C which was not oriented relative to **H**. The other noteworthy feature in Fig. 3 is that above 10 kOe the slope dM/dH for samples A and B is close to that for Cu_2MnSnS_4.

The rapid rise of M at low H is attributed to BMP's associated with holes bound to acceptors. The much slower magnetization rise above 10 kOe is attributed to the d spins outside the BMP's. This interpretation is supported by several arguments, as discussed later. A similar interpretation of magnetization data was given in Refs. 7, 9, 21, and 22.

As noted earlier, all three samples with $x\cong0.9$ exhibited p-type conductivity at room temperatures. In addition, the resistivity of plate C^* rose by four orders of magnitude on cooling from 300 to 2 K and the conduction at low temperatures was characteristic of hopping. These resistivity features indicate that at low T practically all the holes were bound to acceptors. Such bound holes should lead to BMP's. In contrast, the Cu_2MnSnS_4 sample studied in Ref. 20, whose magnetization is also shown in Fig. 3, had high resistivity at room temperature (an insulator). It is not surprising therefore that this sample did not show the characteristic features of BMP's.

In the collective regime each BMP has a sizable net spontaneous magnetic moment. At low T this moment aligns readily in a magnetic field, leading to a fast rise of M at low H. This rapid rise stands out clearly in the present samples because the d spins in the matrix *outside* the BMP align only slowly with H. (The moment per d spin is much smaller than that of the BMP and the d spins interact antiferromagnetically.) As discussed later, approximately 9% of the Mn spins in samples A and B were inside the BMP's, with the remaining 91% in the matrix outside the BMP's. The magnetization of the d spins in the matrix is expected to be similar to that of Cu_2MnSnS_4 with no BMP's.[7]

Figure 4 shows the T dependence of the low-field susceptibility χ of sample A for both $\mathbf{H}\|\mathbf{c}$ (parallel susceptibility) and $\mathbf{H}\perp\mathbf{c}$ (perpendicular susceptibility). Also shown, for comparison, is the low-H susceptibility of the Cu_2MnSnS_4 sample (with no BMP's). The data for Cu_2MnSnS_4 are for $\mathbf{H}\perp\mathbf{c}$, but the values for $\mathbf{H}\|\mathbf{c}$ are similar or even smaller.[20] It is clear from Fig. 4 that at these low temperatures the susceptibility of sample A, for either field direction, is more than an order of magnitude larger than that of a similar sample with no BMP's. The much higher susceptibility is just another manifestation of the rapid alignment of the BMP moment in a field **H**. Similar results were obtained for samples B and C.

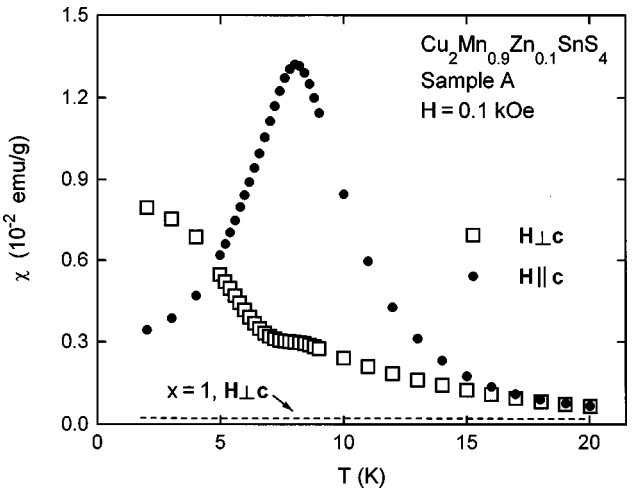

FIG. 4. Temperature dependence of the low-field susceptibility χ in sample *A*, for both $\mathbf{H}\|\mathbf{c}$ and $\mathbf{H}\perp\mathbf{c}$. Also shown, for comparison, is the susceptibility of a sample with $x=1$ and with no BMP's (Ref. 20).

Other noteworthy features in Fig. 4 are (i) a significant difference between the susceptibilities for $\mathbf{H}\|\mathbf{c}$ and $\mathbf{H}\perp\mathbf{c}$ and (ii) ''anomalies'' in the T dependence of χ near 8 K. For $\mathbf{H}\|\mathbf{c}$ the susceptibility exhibits a peak, while for $\mathbf{H}\perp\mathbf{c}$ the curve χ vs T is significantly flatter near 8 K. The temperature 8 K is almost certainly the Néel temperature T_N, where the Mn spins in the matrix order antiferromagnetically. For Cu_2MnSnS_4 ($x=1$), the data of Ref. 20 gave $T_N=8.8$ K. From mean-field theory one expects that T_N is proportional to x, i.e., $T_N=8$ K for the present samples with $x\cong 0.9$.

The boundary between the BMP and the matrix surrounding it is not sharp. The susceptibility data in Fig. 4 imply that the onset of AF order in the matrix affects the BMP susceptibility and its anisotropy. There is therefore an interaction between the matrix and the BMP, and this interaction is probably a major cause of the anisotropy in the BMP. The work on Cu_2MnSnS_4 revealed a magnetic anisotropy below T_N.[20] In the present study the anisotropy in the BMP susceptibility disappears above $2T_N$.

Another possible cause for anisotropy of acceptor BMP's in noncubic materials was considered by Scalbert *et al.*[26] It is related to the anisotropy of the hole and of the *p-d* exchange parameter β. In a wurtzite material the *c* axis becomes the preferred axis for the BMP moment. The matrix in this model is magnetically isotropic (and exhibits no long-range AF order). In the present study, however, the pronounced change in the anisotropy of the BMP susceptibility near T_N (Fig. 4) suggests that the main cause of the BMP anisotropy is the BMP-matrix interaction. The matrix can also affect the interaction between the BMP's themselves. This interaction, which is mentioned later, involves the matrix separating nearby BMP's. A magnetically anisotropic matrix can cause this interaction to depend on the orientation of the magnetic moments of the BMP's. To our knowledge there is no available theoretical treatment of the BMP anisotropy resulting from the matrix anisotropy. A detailed explanation of the BMP anisotropy observed in the present work remains a future challenge.

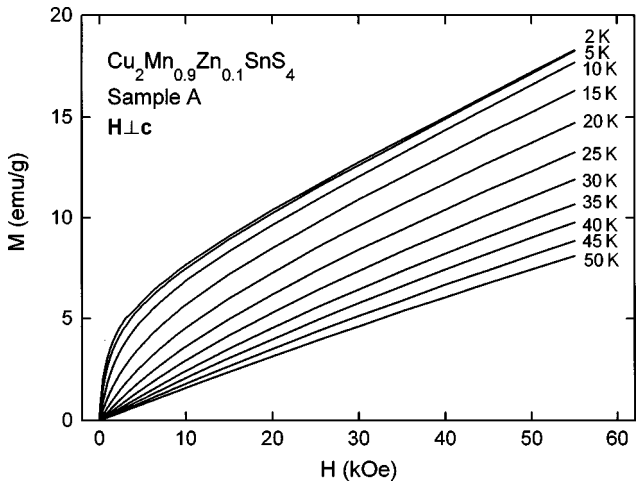

FIG. 5. Isothermal magnetization curves of sample *A*, measured with $\mathbf{H}\perp\mathbf{c}$.

B. Temperature dependence of the magnetization

Figure 5 shows magnetization curves of sample *A* at various temperatures up to 50 K. These data are for $\mathbf{H}\perp\mathbf{c}$. At low temperatures, the fast BMP-magnetization rise can be easily separated from the matrix magnetization. However, as T increases, the BMP magnetization rises more slowly and it becomes more difficult to isolate the BMP contribution to the magnetization. A quantitative analysis that separates the BMP and matrix contributions to M is presented later.

Data for the same sample in the configuration $\mathbf{H}\|\mathbf{c}$ are shown in Fig. 6. Above 10 K the results are similar to those in Fig. 5, but at lower temperatures the AF order in the matrix leads to different features. First, the low-field slope of the magnetization curve decreases as T changes from 10 to 5 to 2 K. This feature is just another manifestation of the susceptibility peak in Fig. 4, for $\mathbf{H}\|\mathbf{c}$. Second, the magnetization curves for 2, 5, and 10 K intersect at higher fields. This is a consequence of the fact, discussed later, that the BMP spontaneous moment increases as T decreases. Thus, although the curve for 2 K starts with a lower slope, it must overtake the other curves at higher fields.

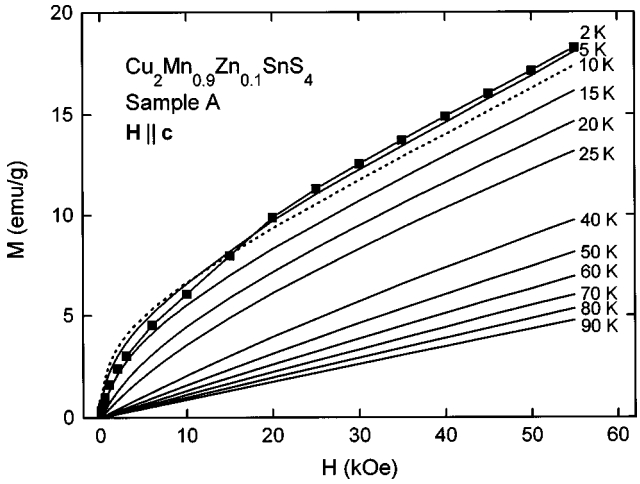

FIG. 6. Isothermal magnetization curves of sample *A*, measured with $\mathbf{H}\|\mathbf{c}$. Data points are shown only for the curve at 2 K. The curve for $T=10$ K is dotted, for clarity.

A close examination of the 2 K data in Fig. 6 shows a vestige of the spin reorientation process (analogous to a spin flop). This process, observed more clearly in Cu_2MnSnS_4,[20] is a property of the matrix. In sample A the spin reorientation is near 15 kOe, compared to 28 kOe for Cu_2MnSnS_4.

Magnetization curves in temperatures up to about 60 K were also obtained for sample B (with both $\mathbf{H}\|\mathbf{c}$ and $\mathbf{H}\perp\mathbf{c}$) and sample C (at one unknown field direction). The data for these samples were less extensive than for sample A, but were otherwise very similar.

C. Analysis of the magnetization curves

A quantitative analysis of the magnetization curves was performed for three purposes: (i) to separate the contribution of the BMP's from that of the matrix, (ii) to find the spontaneous moment m_s of a single BMP, and (iii) to find the concentration of the BMP's. In the collective regime, each BMP has a spontaneous moment m_s that depends on the temperature T. If the number of BMP's is N, then the alignment of the spontaneous moments of all the BMP's leads to a total BMP moment Nm_s. The number N should correspond to the number of occupied acceptors. Based on the resistivity data, practically all acceptors are occupied below 100 K, so that N should be constant at these temperatures.

At the lowest temperatures the total BMP moment Nm_s can be estimated by a linear extrapolation of the high-field portion of the magnetization curve to $H=0$. Such a procedure can be carried out on the data in Fig. 3, for example. However, this intuitive approach is not applicable above 20 K because the separation between the BMP and matrix contributions to M becomes less obvious (see Figs. 5 and 6). Another drawback of a simple extrapolation is that it gives only the product Nm_s, but not N and m_s separately.

The quantitative analysis of the isothermal magnetization curves was based on the equation

$$M = Nm_s\mathcal{L}(m_{\text{eff}}H/k_BT) + \chi_m H, \tag{2}$$

where $\mathcal{L}(x)$ is the Langevin function, k_B is the Boltzmann constant, m_{eff} is an *effective* spontaneous moment per BMP (discussed below), and χ_m is the susceptibility of the matrix. The first term in Eq. (2) represents the contribution of the BMP's. The term $\chi_m H$ is the matrix contribution.

In Eq. (2) a distinction is made between the true and effective spontaneous moments of a BMP, m_s and m_{eff}, respectively. The true spontaneously moment m_s is equal to the magnitude of the aligned moment of a single BMP. On the other hand, the effective moment m_{eff} in the argument of the Langevin function determines how quickly the true moment aligns along $\mathbf{H}$. In an early review by Wolff there was no distinction between m_s and m_{eff} and the BMP magnetization in the collective regime was represented by a Langevin function with $m_{\text{eff}}=m_s$ in its argument.[18] However, in Wolff's more recent work[23] the argument of the Langevin function was changed to $m_sH/k_B(T+T')$. The added temperature T' represents the interaction between the BMP's.[27] Wolff's recent form for the argument of the Langevin function is equivalent to that in Eq. (2), with $m_{\text{eff}}=m_sT/(T+T')$.

In the present work other influences on the BMP, arising from the BMP-matrix interaction, need to be included also. In the following analysis it was *assumed* that a Langevin function having the form in Eq. (2) can account both for the effects of the matrix and for any interaction between BMP's. The good fit that were obtained using Eq. (2) support this approach.

Physically, a larger m_{eff} corresponds to a faster rise of the BMP magnetization with H. Therefore, the susceptibility peak for $\mathbf{H}\|\mathbf{c}$ (Fig. 4) implies high values of m_{eff}. The anisotropy of the low-field susceptibility in Fig. 4, which is evident below 15 K, corresponds to a dependence of m_{eff} on field direction. The relation between m_{eff} and m_s is then more complicated than a simple ratio $T/(T+T')$.

The fitting parameters in Eq. (2) are Nm_s, m_{eff}, and χ_m. To obtain $m_s(T)$ and N separately, we used a procedure based on the following assumption: at sufficiently high temperatures ($T\gg T_N,T'$) the BMP interactions with the matrix and with other BMP's are insignificant compared to the thermal energy. A more explicit statement of this assumption is that at high temperatures m_{eff} (in the argument of the Langevin function) is nearly equal to m_s.

To test the validity of this assumption we imposed the following experimental criteria for the existence of a high-temperature regime where $m_{\text{eff}}\cong m_s$. First, m_{eff}, which is obtained directly from the fit to Eq. (2), should not depend on the direction of $\mathbf{H}$. Second, m_{eff} should not vary from sample to sample. (In a material with a given composition, m_s is a property of the BMP, not of the sample). Third, in any given sample the ratio Nm_s/m_{eff} should be equal to the number N of occupied acceptors and should therefore be independent of T. (It is assumed that the temperature is still low enough that practically none of the acceptors are ionized.) A high-temperature region satisfying these criteria was, in fact, found in the data analysis. The ratio Nm_s/m_{eff} in this region was then used to obtain N for each of the samples. With this N and the values of Nm_s from the fits at different T, the true spontaneous moment per BMP, $m_s(T)$, was obtained.

Before describing the results of the analysis, we discuss the limitations of Eq. (2). The linear term $\chi_m H$ should be a good approximation for the matrix magnetization above T_N. (This statement was verified by a mean-field numerical solution of the magnetization curves between 10 and 50 K, in fields up to 55 kOe). For $T<T_N$, however, the matrix contribution is well approximated by $\chi_m H$ only for $\mathbf{H}\perp\mathbf{c}$, but not for $\mathbf{H}\|\mathbf{c}$. For the latter field direction, spin rotation (analagous to a spin flop) leads to a nonlinear relation between the matrix magnetization and H.[20] For this reason the use of Eq. (1) at $T<T_N$ was restricted to $\mathbf{H}\perp\mathbf{c}$.

There was also an upper limit on the temperature at which Eq. (2) could be used. At sufficiently high T the Langevin function became approximately linear in H, for fields up to 55 kOe. It was then difficult to distinguish between the two terms in Eq. (2). This became evident from the large uncertainties in the fitting parameters. The parameters obtained from the fits were judged to be reliable only below 50 K. Parameters from fits at higher temperature were excluded.

The fits to Eq. (2) described the magnetization curves quite well. An example is shown in Fig. 7. Values of Nm_s (total moment of all the BMP's) obtained from such fits are shown in Fig. 8. For sample A, Nm_s at the lowest T was 5.1 emu/g. The saturation moment M_0 of all the Mn spins in this

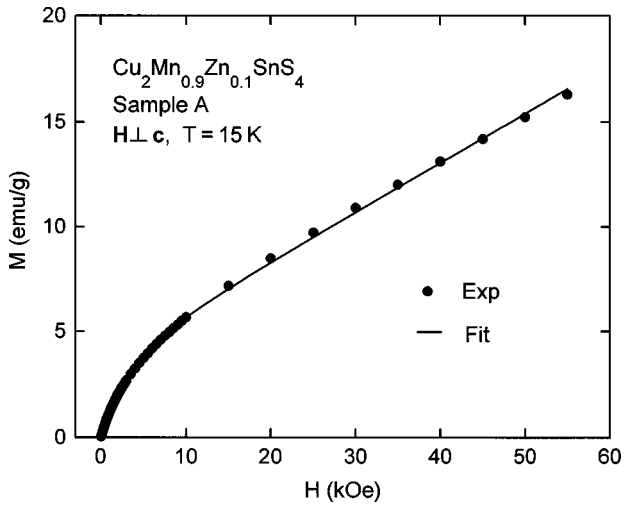

FIG. 7. Example of a fit of an isothermal magnetization curve to Eq. (2). Here the fit is to the data for sample *A* at 15 K and with **H**⊥ **c**.

sample (measured at high fields, as discussed later) was 54 emu/g. Thus approximately 9% of the Mn spins in sample *A* were inside BMP's. The remaining 91% were in the matrix outside the BMP's. These percentages are based, of course, on a simple picture in which there is a sharp boundary between the BMP's and the matrix and in which the spins inside each BMP are saturated at low *T*.

Figure 8 also shows that values for Nm_s in sample *B* were similar to those in sample *A*. For sample *C* the values were only slightly higher. Since Nm_s depends on the number *N* of BMP's, which is also the number of occupied acceptors, it is somewhat surprising that Nm_s was not very sample dependent. Apparently, using the same crystal growth conditions led to similar acceptor concentrations in all the samples.

Figure 9(a) shows $m_{\rm eff}$ as a function of *T* for sample *A*. These results for both **H**∥**c** and **H**⊥ **c** are from fits to Eq. (2). As expected, the anisotropy of the low-field susceptibility

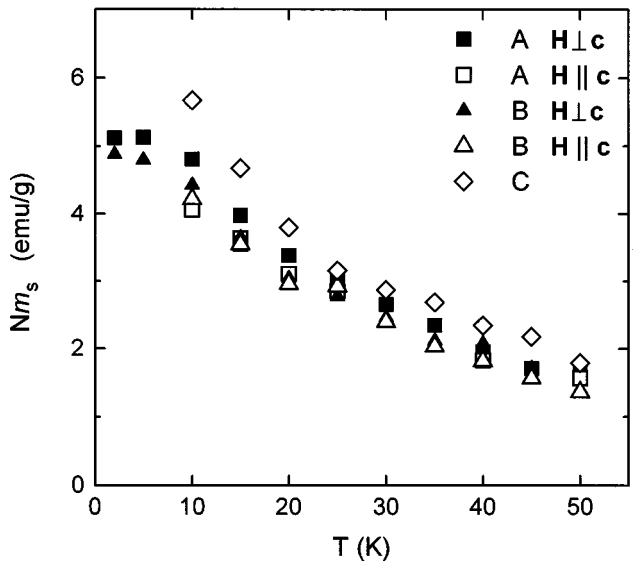

FIG. 8. Values of Nm_s (total moment of the BMP's per gram) obtained from fits of the magnetization curves in samples *A*, *B*, and *C* to Eq. (2).

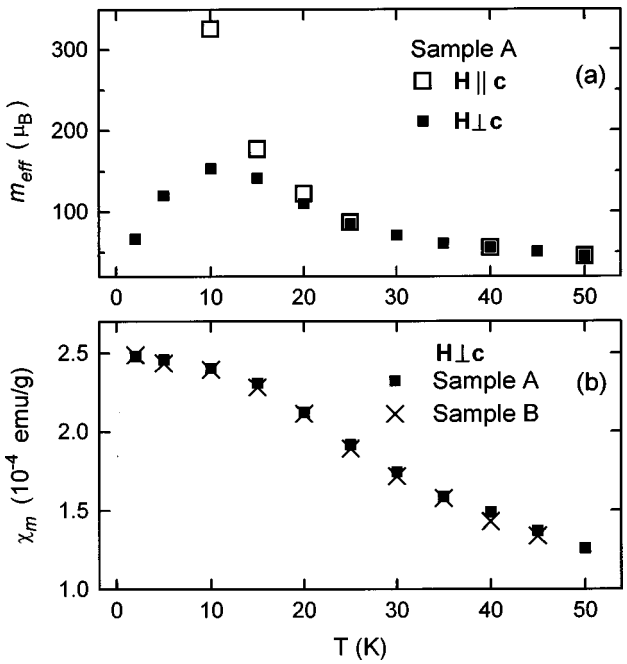

FIG. 9. (a) Effective moment $m_{\rm eff}$ of a single BMP in sample *A*, for both **H**∥**c** and **H**⊥ **c**. (b) Matrix susceptibility χ_m in samples *A* and *B* for **H**⊥ **c**. These results are from fits of magnetization curves to Eq. (2).

(Fig. 4) gives rise to an anisotropy of $m_{\rm eff}$. This anisotropy disappears above 20 K, which suggests that above 20 K $m_{\rm eff}$ in sample *A* is nearly equal to m_s. The results for sample *B* are similar, but in sample *C* with its somewhat higher BMP concentration the anisotropy of $m_{\rm eff}$ disappears only above 30 K. (The result for samples *B* and *C* are not shown.) Very significantly, in the temperature region where $m_{\rm eff}$ is isotropic, the values of $m_{\rm eff}$ in all three samples are practically the same. These results support the basic assumption that $m_{\rm eff} \cong m_s$ at high temperatures.

Additional support for this assumption comes from results for $Nm_s/m_{\rm eff}$. For each sample this ratio is nearly tempera-

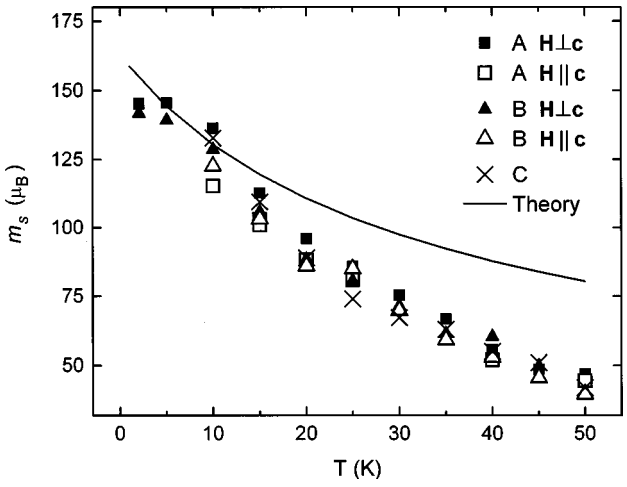

FIG. 10. (True) spontaneous moment m_s of a single BMP as a function of *T*. These results are based on the analysis discussed in the text. The solid curve is from the theoretical simulations in Sec. IV D.

ture independent at the high temperatures where the anisotropy of $m_{\rm eff}$ disappears. Setting $m_{\rm eff}=m_s$ at these temperatures, the average values of $Nm_s/m_{\rm eff}$ for each sample give the following BMP concentrations: $N=(3.8\pm0.2)\times10^{18}$ BMP/g for sample A, $(3.7\pm0.4)\times10^{18}$ BMP/g for sample B, and $(4.6\pm0.3)\times10^{18}$ BMP/g for sample C. These correspond to 1.7×10^{19}, 1.6×10^{19}, and 2.0×10^{19} BMP/cm^3, respectively.

Using these N and the Nm_s in Fig. 8, values for m_s as a function of T were obtained. These results are shown in Fig. 10. The values of m_s in all the samples and for all field directions seem to follow a universal curve. This is consistent with the physical picture in which m_s is an intrinsic property of the BMP and is independent of field direction. The extrapolated value of m_s at $T=0$ is about $143\mu_B$ perBMP. Assuming a moment of $5\mu_B$ per Mn^{2+} ion, this result corresponds to 28.6 Mn ions per BMP. Using a crude model for the BMP, in which all the Mn spins within a sphere of radius R are fully aligned while there is no alignment outside the sphere, one obtains $R=10.7$ Å. Such a radius is comparable to a typical Bohr radius for an acceptor in II-VI materials, which lends further support to the interpretation of the magnetization data in terms of BMP's associated with acceptors.

D. Theoretical modeling

The theoretical modeling followed Ref. 19, as adapted to the present material. The acceptor BMP consists of a hole bound to an acceptor while interacting with the Mn ions via the localized p-d exchange interaction. The acceptor's states investigated by Baldereschi and Lipari include the effects of the complex band structure at the valence-band edge.[28] Here we approximate the acceptor's ground state in the absence of the p-d interaction by a hydrogenic structure with an effective Bohr radius a_0^*. The p-d interaction changes the wave function and the binding energy. It is assumed that the envelope function $\phi(r)$ for the ground state remains spherically symmetric.

The Schrödinger equation for $\phi(r)$ is given by Eq. (15) of Ref. 19. Because the AF interactions between the Mn spins are relatively weak in the stannite structure, the effective Mn concentration $\overline{x}$ that appears in this equation was replaced by the actual concentration x. We used the measured Mn concentration, 88% of the divalent cations. This corresponds to $x=0.22$ in the notation of Ref. 19, in which x is the Mn concentration as a fraction of *all* the cations. The Mn system was treated as paramagnetic, ignoring the AF order of the matrix below 8 K. The magnetic anisotropy of the Mn system was also ignored. The weak AF interactions between the Mn ions were included by replacing the temperature T by an effective temperature $T+T_{\rm AF}$. (The temperature enters into the p-d exchange potential $V_{\rm exch}$ of Ref. 19 via the parameter ξ, which is inversely proportional to T.) The value $T_{\rm AF}=22$ K was chosen based on the estimated Curie-Weiss temperature $\theta=-22$ K. This estimate used the value $\theta=-25$ K for Cu_2MnSnS_4 (Ref. 20) and the proportionality between θ and x.

Several of the material parameters needed for the theoretical modeling were not known. They were chosen as follows. The p-d exchange constant $N_0\beta$ (or N_0J in the notation of Ref. 19) was set equal to the value -0.88 eV in $Cd_{1-x}Mn_xTe$.[29] Two other parameters, the effective Rydberg R_0^* in the absence of the p-d interaction and the dielectric constant ε, were chosen to given an approximate agreement with the measured acceptor binding energy at 300 K (Sec. III) and the experimental value of m_s at 5 K. The chosen values $R_0^*=60$ meV and $\varepsilon=12.76$ lead to a hole effective mass $m^*/m_0=0.718$ and to $a_0^*=9.4$ Å.

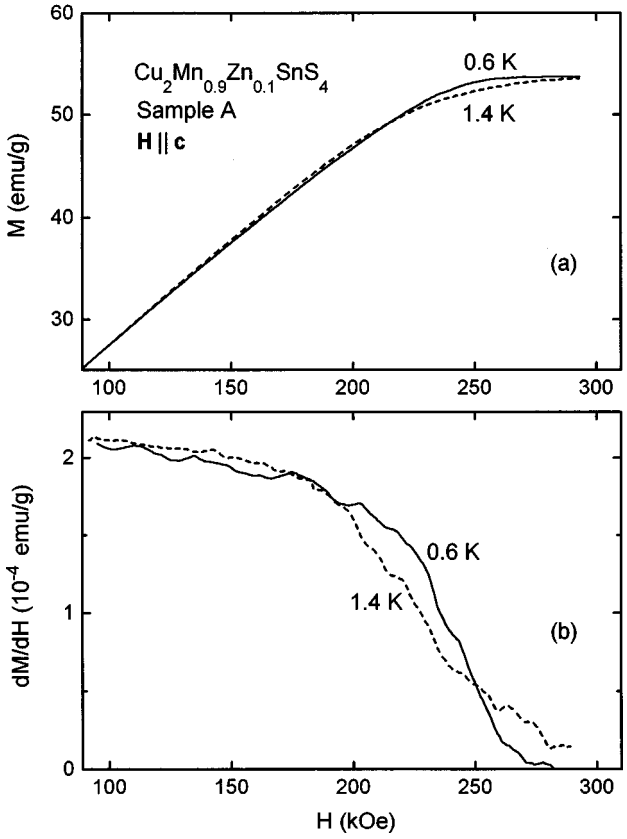

FIG. 11. (a) High-field magnetization of sample A, measured at 0.6 and 1.4 K. (b) Differential susceptibility dM/dH obtained numerically from the data in (a).

The p-d exchange potential is given by Eq. (17) of Ref. 19. The second term in this equation is the fluctuation term.[30] This term is unimportant in the collective regime of the BMP and it did not have a significant affect on the calculated results in the range $T<50$ K where m_s was measured. Nevertheless, the fluctuation term was included in the calculation because it affected the binding energy at 300 K that was used to select the values of R_0^* and ε.

The nonlinear Schrödinger equation for the envelope function $\phi(r)$ was solved numerically by iterative methods.[19] The hydrogenic wave function $\phi(r)\propto\exp(-r/a_0^*)$ was used as an initial guess. The solution for $\phi(r)$ led to many properties of the BMP, including the binding energy and the separate contributions of the Coulomb and p-d interactions to this energy. The spontaneous moment m_s of the BMP was obtained by integrating the correlation function $\langle\mathbf{s}\cdot\mathbf{S}_j\rangle$ between the hole spin $\mathbf{s}$ and the Mn spins $\mathbf{S}_j$, as discussed in Ref. 19. All the calculations were only for $H=0$.

Figure 10 compares the calculated T dependence of m_s with the experimental values. There is qualitative agreement,

although, clearly, the calculated values decrease less rapidly with increasing T. It is believed that a major cause of the discrepancy is the choice of a hydrogenic wave function for the acceptor, which did not take into account the actual band structure. In addition, although the chosen material parameters $N_0\beta$, R_0^*, and ε, are reasonable, they may not be accurate. More realistic theoretical simulations of the BMP remain a future challenge.

E. Magnetic behavior of the matrix

The temperature variation of the matrix susceptibility χ_m in the configuration $\mathbf{H}\perp\mathbf{c}$ is shown in Fig. 9(b). These results are from the fits to Eq. (2). The temperature variation of χ_m is weaker below the Néel temperature of the matrix, $T_N=8$ K. The values of χ_m are comparable to those in the Cu_2MnSnS_4 sample with no BMP's,[20] as expected.

The high-field canted-to-paramagnetic phase transition was studied in sample A using a 300-kOe hybrid magnet. The magnetization data are shown in Fig. 11(a) and the derivative dM/dH in Fig. 11(b). The observed phase transition is more rounded than in the Cu_2MnSnS_4 sample with no BMP's.[20] A more rounded transition in samples with BMP's was observed earlier in EuTe.[7] The transition field in Fig. 11, about 225 kOe for $T=1.4$ K, is slightly lower than that in Cu_2MnSnS_4.[20] Such a lower transition field is consistent with mean-field theory,[31] which predicts a transition field proportional to x. The saturation moment in Fig. 11(a) is $M_0=54$ emu/g.

ACKNOWLEDGMENTS

We are grateful to P.A. Wolff for many useful discussions and for a copy of his work, prior to publication. We are also thankful to P. Belca for making the electrical contacts for the resistivity measurements. The work at Tufts University was partially supported by NSF Grant No. DMR-9219727. The work at Brown University was supported by NSF Grant No. DMR-9221141. The Francis Bitter National Laboratory was supported by NSF.

*Deceased.

[1] S. Methfessel and D. C. Mattis, in *Magnetism*, edited by S. Flügge, Handbuch der Physik Vol. XVIII/1 (Springer, Berlin, 1966), p. 389ff.

[2] *Semimagnetic and Diluted Magnetic Semiconductors*, edited by M. Averous and M. Balkanski (Plenum, New York, 1991).

[3] *Diluted Magnetic Semiconductors*, edited by J. K. Furdyna and J. Kossut, Semiconductors and Semimetals Vol. 25 (Academic, New York, 1988).

[4] S. von Molnar and S. Methfessel, J. Appl. Phys. **38**, 959 (1967).

[5] A. Yanase and T. Kasuya, J. Phys. Soc. Jpn. **25**, 1025 (1968).

[6] E. L. Nagaev, Zh. Éksp. Teor. Fiz. **54**, 228 (1968) [Sov. Phys. JETP **27**, 122 (1968)]; Usp. Fiz. Nauk **117**, 437 (1975) [Sov. Phys. Usp. **18**, 863 (1976)].

[7] N. F. Oliveira, Jr., S. Foner, Y. Shapira, and T. B. Reed, Phys. Rev. B **5**, 2634 (1972;).

[8] Y. Shapira, S. Foner, N. F. Oliveira, Jr., and T. B. Reed, Phys. Rev. B **5**, 2647 (1972).

[9] J. Vitins and P. Wachter, Solid State Commun. **13**, 1273 (1973); Phys. Rev. B **12**, 3829 (1975).

[10] Y. Shapira, S. Foner, N. F. Oliveira, Jr., and T. B. Reed, Phys. Rev. B **10**, 4765 (1974).

[11] S. von Molnar, A. Briggs, J. Flouquet, and G. Remenyi, Phys. Rev. Lett. **51**, 706 (1983); J. Stankiewicz, S. von Molnar, and F. Holtzberg, J. Magn. Magn. Mater. **54-57**, 1217 (1986).

[12] E. L. Nagaev, J. Magn. Magn. Mater. **110**, 39 (1992); Phys. Status Solidi B **186**, 9 (1994).

[13] A. Mauger and C. Godart, Phys. Rep. **141**, 51 (1986).

[14] M. Umehara, Phys. Rev. B **46**, 12 323 (1992); **54**, 5523 (1996).

[15] T. Dietl and J. Spalek, Phys. Rev. Lett. **48**, 355 (1982).

[16] D. Heiman, P. A. Wolff, and J. Warnock, Phys. Rev. B **27**, 4848 (1983).

[17] A. K. Ramdas and S. Rodriguez in *Diluted Magnetic Semiconductors* (Ref. 3), p. 345ff.

[18] P. A. Wolff, in *Diluted Magnetic Semiconductors* (Ref. 3), p. 413ff.

[19] L. R. Ram-Mohan and P. A. Wolff, Phys. Rev. B **38**, 1330 (1988).

[20] T. Fries *et al.*, Phys. Rev. B **56**, 5424 (1997).

[21] Y. Shapira, E. J. McNiff, Jr., N. F. Oliveira, Jr., E. D. Honig, K. Dwight, and A. Wold, Phys. Rev. B **37**, 411 (1988).

[22] D. X. Li, Y. Haga, H. Shida, T. Suzuki, T. Koide, and G. Kido, Phys. Rev. B **53**, 8473 (1996).

[23] P. A. Wolff (unpublished). This work analyzes unpublished data of J. Liu on p-type $Zn_{0.95}Mn_{0.05}Te$.

[24] T. Wojtowicz, S. Kolesnik, I. Miotkowski, and J. K. Furdyna, Phys. Rev. Lett. **70**, 2317 (1993).

[25] B. I. Shklovskii and A. L. Efros, *Electronic Properties of Doped Semiconductors* (Springer, Berlin, 1984).

[26] D. Scalbert, M. Nawrocki, C. Benoit à la Guillaume, and J. Cernogora, Phys. Rev. B **33**, 4418 (1986).

[27] P. A. Wolff, R. N. Bhatt, and A. C. Durst, J. Appl. Phys. **79**, 5196 (1996).

[28] A. Baldereschi and N. O. Lipari, Phys. Rev. B **3**, 439 (1971).

[29] J. A. Gaj, R. Planel, and G. Fishman, Solid State Commun. **29**, 435 (1979).

[30] J. Warnock and P. A. Wolff, Phys. Rev. B **31**, 6579 (1985).

[31] F. G. Brady Moreira, I. P. Fittipaldi, S. M. Rezende, R. A. Tahir-Kheli, and B. Zeks, Phys. Status Solidi B **80**, 385 (1977).